

# Multibody interactions of actuated magnetic particles used as fluid drivers in microchannels

R. J. S. Derks · A. J. H. Frijns · M. W. J. Prins ·  
A. Dietzel

Received: 26 November 2009 / Accepted: 30 November 2009 / Published online: 24 December 2009  
© The Author(s) 2009. This article is published with open access at Springerlink.com

**Abstract** The forced motion of superparamagnetic particles and their multibody interactions are studied in view of the application as integrated fluid drivers in microchannel systems. Previous studies on particle manipulation in open fluid volumes serve as our starting point for the analysis of particle dynamics and interplay effects in confined fluid volumes. An experimental setup is designed that offers a constant force field on all individual particles dispersed in a microchannel. Distinguishable multi-particle configurations are observed and analyzed on the basis of magnetic and hydrodynamic particle interaction mechanisms. The fluid driving performance and the efficiency of the particles are evaluated on system level by means of numerical simulation models.

**Keywords** Confined superparamagnetic particles · Microchannel systems · Magnetic and hydrodynamic interactions · Integrated fluid actuation · Magnetic field shaping · Isodynamic force field

---

R. J. S. Derks (✉) · A. J. H. Frijns · A. Dietzel  
Mechanical Engineering, Eindhoven University of Technology,  
P.O. Box 513, 5600 MB Eindhoven, The Netherlands  
e-mail: r.j.s.derks@tue.nl

M. W. J. Prins  
Applied Physics, Eindhoven University of Technology,  
P.O. Box 513, 5600 MB Eindhoven, The Netherlands

M. W. J. Prins  
Philips Research Europe, High Tech Campus 12,  
5656 AE Eindhoven, The Netherlands

A. Dietzel  
Holst Centre, High Tech Campus 31, 5605 KN Eindhoven,  
The Netherlands

## 1 Introduction

The current trend in lab-on-a-chip devices involves the miniaturization and integration of a wide range of functions (Haeberle and Zengerle 2007). For biosensors, a main challenge lies in achieving a high functional performance with respect to sensitivity, specificity, and speed (Bruls et al. 2009). Devices for biochemical analysis therefore often contain elements with a large surface area to enhance binding capacity and allow parallel screening. For instance, porous DNA hybridization microarrays have become an effective form of screening technology and allow the analysis of hundreds to thousands of genes simultaneously (Chen et al. 2007; Grasso et al. 2006). A concern in these high-surface area systems is the limited accessibility of the reactive surfaces for the fluid and analyte, which slows down the effective reaction rate (Vanderhoeven et al. 2005; Yuen et al. 2003). As an example, we consider a porous structure with microchannels of length  $L$  of several hundreds of micrometers. Assuming molecular diffusion only, the time  $\tau$  required to travel the distance  $L$  can be estimated using Einstein's law of diffusion (Vanderhoeven et al. 2005):  $\tau = L^2 / (2 \cdot D)$ . A DNA molecule or protein with a typical diffusion coefficient  $D$  of  $10^{-11}$  m<sup>2</sup>/s needs hours to travel from the channel inlet to the outlet. Furthermore, only a fraction of the molecules is able to enter the pore that holds the specific capture molecules on its surface. Active transportation of fluid and analyte within and through micropores is therefore essential to enable accelerated reaction rates. Several actuation methods have already been discussed in literature, but each having one or more crucial shortcomings. External mechanical pumps typically require large sample volumes (Vanderhoeven et al. 2005; Yuen et al. 2003; Laser and Santiago 2004). Open systems such as droplet-based actuation are sensitive

to evaporation (Gutmann et al. 2005). Systems based on capillary or electro kinetic flows have a strong dependence on the chemical properties of the sample (Vanderhoeven et al. 2005; Laser and Santiago 2004). In fact, a fluid actuation system for high-surface-area elements should be fully integrated and suited for small samples of complex biological fluids (Chen et al. 2007).

Superparamagnetic particles can be used for different functions in lab-on-a-chip applications (Gijs 2004; Pamme 2006; Bruls et al. 2009). Their electromagnetic motion control is very flexible and can even be combined with the self-assembly and alignment of particle chains (Derks et al. 2007; Petousis et al. 2007). As biological materials are essentially non-magnetic, functions such as sample filtering, analyte transport, mixing, labeling, or detection can be applied in complex samples without undesired side effects and high reproducibility. In this paper, we propose a novel way for integrated fluid transport in porous high surface area systems based on the hydrodynamic momentum transfer by magnetic particles. By means of applied magnetic fields, the particles are actuated in the microchannels in a non-contact approach. The fluid is driven by the forced motion of the particles to create a net flow through the pores, as illustrated in Fig. 1. Such integrated driving mechanism can be applied in a porous system for large as well as small sample volumes, without generating dead fluid volumes. Several papers have addressed the use of magnetic particles for fluidic pumping on the microscale (Hatch et al. 2001; Hartshorne et al. 2004). These discuss irreversibly aggregated plugs of enormous numbers of

ferromagnetic nano-particles in water that are controlled as an entity only. The proposed systems are hard to match to microchannel dimensions, and harmonization of particle to channel dimensions is not considered. Moreover, most published research considers the dynamics of particles either following a simplistic single particle approach, or describes the particle ensemble as a continuum (Ganguly et al. 2005). The particle-to-particle interactions are not considered in detail, although these affect the dynamics of the particles and the particle loaded fluid. Especially the hydrodynamic momentum transfer from a particle to the fluid (and from there back to neighboring particles) is often neglected, but can be dominant over magnetic particle interactions (Derks et al. 2008; Mikkelsen et al. 2005; Mikkelsen and Bruus 2005). To understand the influence of local magnetic and hydrodynamic particle interactions, we first summarize particle dynamics effects in open fluid volumes. For our further experimental study we have designed a setup to track the dynamics of particles confined in microchannels, where the particle radius and channel radius differ less than an order of magnitude. The experimentally obtained particle configurations are analyzed by means of numerical simulations considering the mechanisms of magnetic and hydrodynamic interactions and are finally evaluated in view of the application as integrated fluid drivers with system parameters such as fluid outflow, pump efficiency, and the required pressure drop.

## 2 Particle dynamics in open fluid volumes

Several papers already discussed the dynamics of single particles and self-assembled chains in large open fluid volumes (Pamme 2006; Derks et al. 2007; Petousis et al. 2007), as we will summarize in this section. Micrometer-sized particles that are typically used in lab-on-a-chip systems are large enough to be minimally disturbed by Brownian motion (actuation energy dominates over thermal energy). The small length scales and low particle velocities result in a pure laminar flow ( $Re \ll 1$ ). Under these approximations, the velocity of a single superparamagnetic particle  $\vec{v}_{p,\text{free}}$  induced by a magnetic force  $\vec{F}_m$  can be expressed as (Derks et al. 2007)

$$v_{p,\text{free}} = \frac{\vec{F}_m}{6 \cdot \pi \cdot \eta \cdot r} = \frac{\chi_p \cdot r^2}{9 \cdot \mu_0 \cdot \eta} \vec{\nabla} B^2 \quad (1)$$

The particle is assumed to be magnetized proportional to the effective magnetic susceptibility  $\chi_p$  and is driven by the gradient of the squared magnetic induction  $\vec{\nabla} B^2$ . Its velocity depends on the squared radius of the particle  $r^2$ . The dynamic viscosity of the surrounding fluid is represented by  $\eta$ , and  $\mu_0$  is the magnetic permeability of vacuum:  $4\pi \cdot 10^{-7}$  H/m. Two or more superparamagnetic

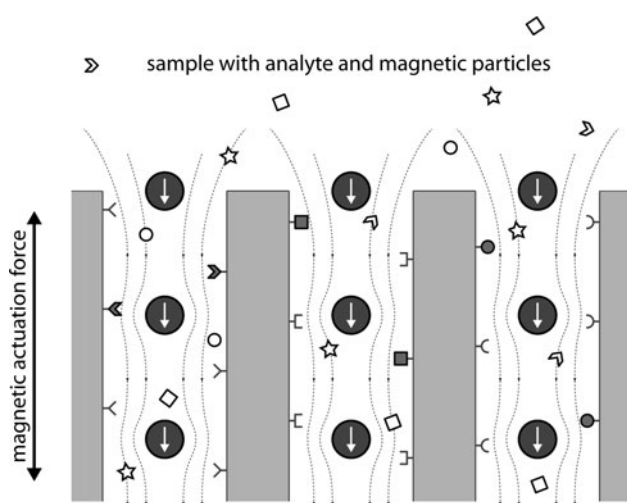


**Fig. 1** A sketch of the fluid driving concept in microchannels by confined actuated superparamagnetic particles. The particles (indicated as *black spheres*) travel through the pores under the action of external magnetic fields (indicated by the *white arrows*), thereby inducing drag forces on the fluid (and dissolved analyte) that generate a flow in the channel (indicated by the *dashed streamlines*)

particles that get in proximity will influence each other by multiple interactions. For the case of magnetic interplay, the dipole–dipole interaction force  $F_{m,int}$  between two particles, induced by its magnetic moment  $m$  that is aligned with the magnetic field, is given by (Mikkelsen et al. 2005)

$$F_{m,int} = \frac{\mu_0 \cdot m^2}{4 \cdot \pi \cdot s^4} = \frac{4 \cdot \pi \cdot r^6 \cdot \chi_p \cdot B^2}{9 \cdot \mu_0 \cdot s^4} \tag{2}$$

In addition to magnetic interactions, particles also influence each other by hydrodynamics. The (magnetic) driving force on a particle is balanced by viscous forces from the fluid, transferring momentum to the fluid and subsequently to a nearby particle. In order to explain this interaction, we consider the one-dimensional flow profile of the fluid induced by a particle in motion on an imaginary travel axis (Happel and Brenner 1973)

$$\vec{v}_f = \vec{v}_{p,free} \cdot \left( \frac{3}{2} \cdot \left( \frac{r}{s+r} \right) - \frac{1}{2} \cdot \left( \frac{r}{s+r} \right)^3 \right) \tag{3}$$

The induced fluid velocity profile by two particles in their travel direction can be calculated by superposing the two corresponding velocity profiles. A first order approximation of the hydrodynamic interaction forces between identical magnetic particles can be estimated with (Derks et al. 2008)

$$\vec{F}_{f,int} = \frac{r \cdot \vec{F}_m \cdot (3 \cdot s^2 + 6 \cdot s \cdot r + 2 \cdot r^2)}{2 \cdot (s+r)^3} \tag{4}$$

Hydrodynamic interactions between particles in close proximity are not as strong as the magnetic interactions, but will already dominate a few particle diameters away because of the slower  $s^{-1}$  decline, as shown in Fig. 2. Furthermore, hydrodynamic interaction forces work in the same direction as the common motion of both particles. On the other hand, magnetic particle–particle interactions can be attractive or repulsive depending on their orientation with the magnetic field, and can also have another direction than the actuation force given by the magnetic gradient direction. Magnetic particles can also aggregate into chains by these magnetic interactions that require a different velocity calculation due to their physical contact and the shape elongation, defined by the ratio between the chain length  $l$  and particle radius  $r$ . Magnetic interactions between neighboring particles induce a chain magnetization enhancement  $\alpha_m$ , which is approximated in simulations to be 1.2 (Derks et al. 2007). The hydrodynamic drag is also influenced by the chain aspect ratio, and is expressed with constants  $C_1$  and  $C_2$  that are determined in experiments to be 9 and 0.56, respectively. The velocity of an actuated magnetic particle chain in an open fluid volume  $\vec{v}_{c,free}$  is expressed as (Derks et al. 2007)

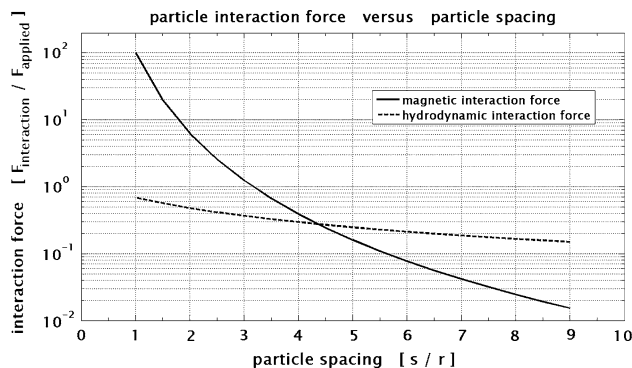


**Fig. 2** A comparison of magnetic and hydrodynamic interaction forces ( $F_{interaction}$ ) between two 20  $\mu\text{m}$  particles, which travel along an imaginary axis in an open fluid volume under the action of a magnetic field gradient ( $F_{applied}$ ). Magnetic interactions are strong, but fall off very quickly as a function of the particles interspacing ( $s$ ). The hydrodynamic interaction force falls off much slower and already dominates from a spacing of a couple of particle radii ( $r$ ) on

$$\vec{v}_{c,free} = \left( \frac{(\ln(l/r) + C_2) \cdot \alpha_m}{1/6 \cdot C_1} \right) \cdot \vec{v}_{p,free} \tag{5}$$

### 3 Particle experiments in microchannels

In a microchannel system, the magnetic particles are in close proximity to no-slip boundaries, which changes the particle motion in terms of direction and velocity compared to the case of particles in an unbound fluid. The effects of this so-called particle confinement are complex and difficult to predict with analytical methods. A setup was built to experimentally study the motion and interplay of superparamagnetic particles in a microchannel under constant magnetic driving force conditions, as shown in Fig. 3. It consists of a PVC frame (80 mm by 80 mm), a polycarbonate (PC) fluidic chip (8 mm by 8 mm), and a magnetic system with a copper wire solenoid (4 cm in width), and two precisely shaped soft-magnetic yokes (ARMCO, AK Steel, The Netherlands) for particle actuation. In the fluidic chip, a microchannel with square cross section was created by excimer laser ablation (Micro Master, Optec, Frameries, Belgium). The chip is exchangeable so that different channel dimensions could be studied, ranging from 1 to 5 mm in length and from 10 to 250  $\mu\text{m}$  in width. The microchannel in- and outlet were coupled by two large backflow channels (total cross section 2  $\text{mm}^2$ ) to minimize external pressure drops. The entire chip was completely sealed using a thin lid of poly carbonate and disconnected from any external device. The particles were dispersed in the microchannel, where the fluid was density-matched with the particles to compensate for gravitational influences [ $\rho = 1500 \text{ kg/m}^3$ , for procedure see Derks et al. (2007)]. An optical microscope (Olympus, BX51) was used

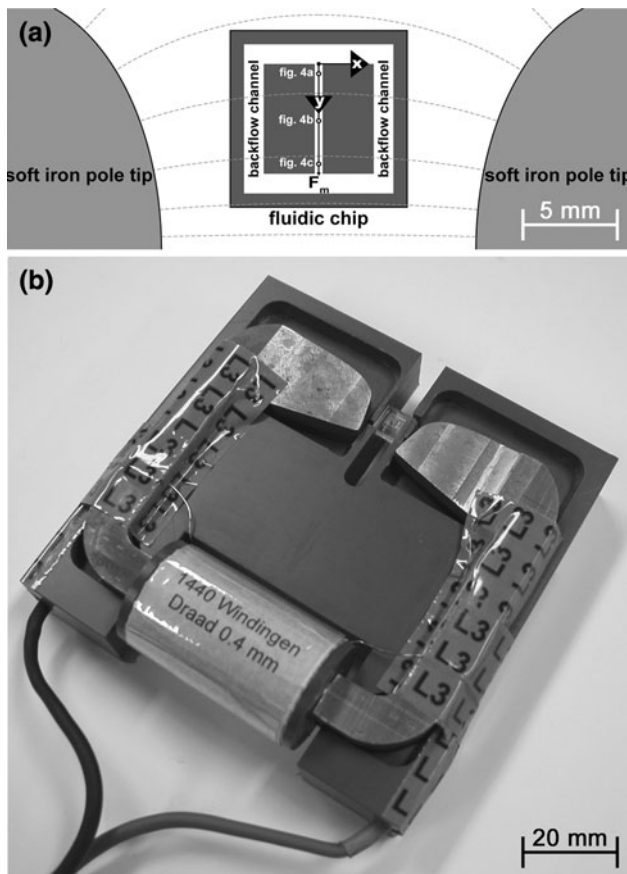


**Fig. 3** The experimental setup that produces an isodynamic force field over particles traveling through a microchannel along the  $y$ -axis. The gradient of the magnetic field decreases along the channel ( $y$ -axis from top to bottom), but is compensated by an increasing field amplitude, resulting in a constant  $\vec{\nabla}B^2$  (a). The device achieves about  $0.25 \text{ T}^2/\text{m}$  with only  $50 \text{ mT}$  as maximum field to ensure that particles are linearly magnetized proportional to their susceptibility, at a current of  $1 \text{ A}$  through the solenoid (b)

to visualize the motion of individual particles down to  $1 \mu\text{m}$  in diameter.

To achieve independent observation of the magnetic and hydrodynamic interactions the magnetic field was shaped to follow certain requirements: The magnetic field lines are oriented perpendicular to the channel axis to magnetize the particles perpendicular to their direction of motion, and have the least correlation with the hydrodynamic interactions in axial direction. To study multiple particle configurations, the main condition is a constant driving force on each particle. The value of  $\vec{\nabla}B^2$  has to be constant (Eq. 1), meaning that the absolute value of the magnetic induction  $B$  has to balance with the value of the field gradient  $\vec{\nabla}B$  over the center of the microchannel along the  $y$ -axis

$$\vec{\nabla}B^2 = 2B \cdot \vec{\nabla}B = \text{const.} \quad (6)$$

For a gradient having a non-zero value,  $B$  becomes a function of the channel length at the  $y$ -axis. The pole pieces

shape illustrated in Fig. 3 result in a decrease in the magnetic field and an increasing gradient along the centerline of the channel ( $x = 0$ ). Because the field lines are horizontal when arriving at the channel axis, only the  $x$ -component of  $B$  is of influence. By an integration step, the required magnetic field at the centerline of the channels can be expressed as

$$\vec{B}_x = \sqrt{2 \cdot \vec{\nabla}B^2 \cdot y + B_{y=0}^2} \quad (7)$$

The pole pieces were made of high permeability, linear, and isotropic material. Hence, there are no tangential components for  $B$  at the pole surfaces, and can therefore be assumed to be equipotential surfaces. With Eq. 7, the Maxwell equations and the ratio  $f = \vec{\nabla}B^2/B_{y=0}^2$ , the shape of the pole pieces was analytically calculated to be (Chalmers et al. 1999)

$$x = \pm \frac{\sin^{-1}(e^{f \cdot y} \cdot \sin(f \cdot x_0))}{f} \quad (8)$$

Numerical simulations of the above solution indicated that end-effects have a strong influence on the uniformity and length of the isodynamic force field. An iterative optimization on the tip ends was carried out numerically with Eq. 8 as initial condition, in order to extend the isodynamic force field as much as possible. Optimization resulted in a full coverage of the largest channel dimensions (length  $5 \text{ mm}$ ) allowing  $10\%$  variation in magnetic force, which is already more accurate than the particle-to-particle variations (Derks et al. 2007; Van Ommering et al. 2009). The height of the pole pieces was set to  $10 \text{ mm}$ , equal to twice the channel length. To be able to fit in the fluidic chip, the minimum separation  $x_0$  between the pole pieces was set to  $10 \text{ mm}$ . The value of  $\vec{\nabla}B^2$  was set to be around  $0.1 \text{ T}^2/\text{m}$  for sufficient magnetic driving forces. The value of the maximum magnetic field did not exceed  $50 \text{ mT}$  to stay in the linear regime of the particle magnetization curve (Derks et al. 2007). To minimize the risk of magnetic saturation, the cross-sectional area of the yokes were maximized where possible. The final shape achieved about  $0.25 \text{ T}^2/\text{m}$  with a maximum field of only  $50 \text{ mT}$  using a current of  $1 \text{ A}$  through the solenoid, measured with a Gauss probe fitted on an  $x$ - $y$  stage.

Figure 4 shows different configurations of  $20 \mu\text{m}$  superparamagnetic particles (Sphero, Spherotech, USA) with  $\chi_p = 0.06$  (measured by VSM measurement) traveling with velocities in the order of  $100 \mu\text{m}/\text{s}$  under the action of the magnetic field with  $\vec{\nabla}B^2 = 0.1 \text{ T}^2/\text{m}$ , in a  $4 \text{ mm}$  long channel of  $100 \mu\text{m}$  in width and depth. In panel (a), the particles experienced a low field intensity of  $10 \text{ mT}$  ( $y = 0$ – $1 \text{ mm}$ , top of the setup). The hydrodynamic forces dominated over the magnetic interactions that were weak,



and the particles lined up on the channel axis owing to the focusing effect induced by the channel walls. In this axially aligned configuration, the dipolar magnetic interactions resulted in small repelling forces between the particles. Successively, the particles self organized in a spread poly-twin configuration (Derks et al. 2008). Panel (b) shows an ensemble of particles that experience a magnetic field of 25 mT ( $y = 2$  mm, halfway the channel). The particles leave their common central motion axis due to the increasing magnetic interaction forces stimulating the particles to form chains aligned with the field lines. In panel (c), the particles are observed in the position of the highest magnetic field setting of 50 mT ( $y = 3$ –4 mm, bottom of the setup), where the particles are fully aggregated into chains and oriented perpendicular to their motion direction. The chains repel each other in axial direction, similar to the case of the particle twins in panel (a), and the chain length was limited by the channel confinement. Although two stable configurations could be clearly distinguished as shown in Fig. 4a, c, the particles require a transition length before equilibrating in a new configuration.

#### 4 Numerical simulations

In order to analyze the observed configurations of the confined particles on the basis of multibody interaction phenomena and their related fluid driving performance, two numerical simulation models have been developed using Comsol Multiphysics. In the first model, particles aligned and traveling along the channel axis (as the case of Fig. 4a) are studied by a two-dimensional axi-symmetric model. The second and more complicated configuration of particle chains, centered but oriented perpendicular to their motion direction (as the case of Fig. 4c) is studied by a full three-dimensional model. In both models, a microchannel with no-slip boundaries is assumed with radius  $R$  and length  $L = 100 \cdot r$ , and is filled with fluid with density  $\rho$  of  $1000 \text{ m}^3/\text{kg}$  and viscosity  $\eta$  of  $1 \text{ mPa s}$ . The spherical particles with radius  $r$  are modeled as individual domains with a several orders of magnitude higher viscosity, in order to take into account all effective body forces. Assuming an identical effective susceptibility  $\chi_p$ , every particle experiences a force of  $F = 20 \text{ fN}$  in axial direction (calculated using Eq. 1 and assuming the experimental average particle velocity of  $100 \text{ }\mu\text{m/s}$ ). As in the experiments, the fluid flow is purely laminar ( $Re \ll 1$ ) and Brownian motion can be neglected for the particle sizes that were used. In this regime, the models are fully scalable and results are therefore normalized to the particle radius or the single particle velocity in an open fluid volume.

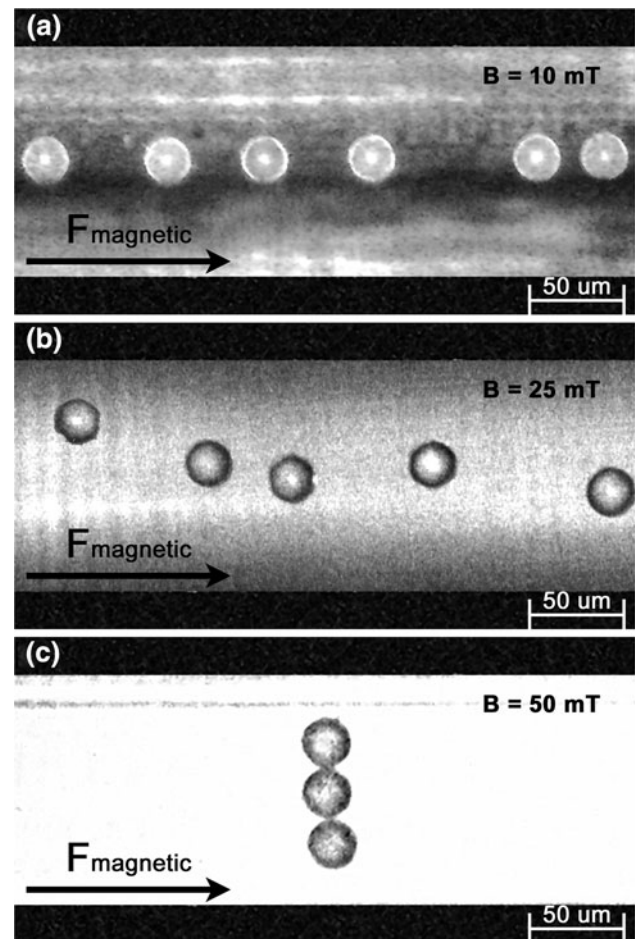


**Fig. 4** Magnetic particles ( $\varnothing = 20 \text{ }\mu\text{m}$ ) traveling with velocities in the order of  $100 \text{ }\mu\text{m/s}$ , in a 4 mm long channel of  $100 \text{ }\mu\text{m}$  in width and depth, under the action of a magnetic field gradient with  $0.1 \text{ T}^2/\text{m}$ . All snapshot locations are indicated in Fig. 3a. At the top of the channel ( $y = 0 \text{ mm}$ ,  $B = 10 \text{ mT}$ ), the channel walls induce a focusing effect on the particles that leads to a poly-twin configuration (Derks et al. 2008) (a). With a higher field amplitude and lower field gradient halfway the channel ( $y = 2 \text{ mm}$ ,  $B = 25 \text{ mT}$ ), particles reorganize in less ordered configurations (b). At the channel bottom the field intensity is high ( $y = 4 \text{ mm}$ ,  $B = 50 \text{ mT}$ ), and particles aggregate into chains aligned with the field lines perpendicular to the travel direction (c)

##### 4.1 Particle configuration analysis

At first, both numerical models are used to find the theoretical transition regime for the two stable particle configurations. The transformation to a certain configuration is triggered by a set of different forces acting on the particles. Similar to the dynamics in open fluid volumes, simulations accounted for the external magnetic driving forces (Eq. 1), hydrodynamic interaction forces (Eq. 4), and magnetic dipole interaction forces (Eq. 2). In this special case of the particles and fluid being confined by the channel, also hydrodynamic focusing forces induced by the channel walls had to be considered. As a consequence of the

isodynamic force field, the magnetic driving force on every individual particle and its resulting velocity in axial direction was assumed to be constant over the entire channel. The hydrodynamic focusing force from the wall is proportional to the particle velocity and could also be assumed constant (Happel and Brenner 1973). The same applies for the hydrodynamic interaction forces, assuming that the particle spacing does not vary. The magnetic dipole interaction is the only particle force that varies with the magnetic field along the channel length. As can be derived also from Eq. 2, the experimental shift from 10 to 50 mT gives approximately 25 times stronger magnetic particle interaction forces, which eventually forced the particles to assemble in chains perpendicular to their motion direction. Assuming the particles could reorder instantaneously from the axial aligned configuration (Fig. 4a) to the perpendicular chain configuration (Fig. 4c), the simulation models estimated a transition point of about 21 mT where the magnetic interaction forces start to dominate over the hydrodynamic focusing forces. The calculations match with the experiments where the transition was observed between 10 and 50 mT, but are highly influenced by the initial particle configuration and particle spacing.

#### 4.2 Driving fluids in axial configurations

The axi-symmetric simulation is used to study the velocity of particles lined up along the channel axis. The particle-to-channel radius ratio is being varied. Hydrodynamic interactions with the channel wall force the particles (or chain) to slow down. Longer chains move faster in a channel, similar to the case of chains in open fluid volumes (Eq. 5). A first order approximation of the velocity of a confined particle or chain can be fitted to the simulations

$$\vec{v}_{c,\text{confined}} = \left( \frac{R-r}{R+r} \right) \cdot \vec{v}_{c,\text{free}} \quad (9)$$

The fluid outflow is the most important parameter to describe the pump performance of the magnetic particles acting as fluid drivers. The volume of the particles present in the channel is subtracted from the calculated outflow to obtain the pure fluid flow. The simulation results are based on the axi-symmetric model where only one channel is considered. To reflect the case of a multi-channel system, the obtained volumetric flow rate is divided by the channel cross-sectional area to obtain the average fluid velocity, as smaller channel diameters allows for more channels on the available system surface. A high fluid flow is reached if particles reach a reasonable velocity itself, but should on the other hand create sufficient drag on the surrounding fluid. By varying the channel to particle radius, simulations reveal the highest effective fluid flow at  $R/r$  between 5 and 10, shown in Fig. 5a. Next, the influence of possible

particle spacing is studied. In the axi-symmetric model, the radius ratio is now fixed at  $R/r = 5$ . Spreading the particles reduces the exchange of momentum between particles leading to lower particle velocities, but increases the fluid drag per particle. These effects compensate each other beyond  $s \geq 5 \cdot r$ , and the resulting fluid outflow is therefore not affected. The spreading only influences the particle residence time in the channel, and therefore affects the pump efficiency per particle expressed as the ratio between the induced fluid velocity and the particle velocity  $\bar{v}_f/\bar{v}_p$ , illustrated in Fig. 5b. If more particles are added to the system, both the pump performance and pump efficiency increase proportionally to the number of particles. The fluid velocity can then exceed 10% of the average particle velocity. A problem in microfluidics is the enormous the pressure drop required to reach reasonable fluid velocities. For a pressure driven system described by the law of Poiseuille, linearly downsizing the channel diameter results in a quadratic increase of the required pressure over the channel to maintain the same average fluid velocity (Happel and Brenner 1973)

$$\bar{v}_{f,\text{avg}} = \frac{\Delta p \cdot R^2}{8 \cdot \eta \cdot L} \quad (10)$$

Figure 5c represents the maximum values of the particles-induced pressure drop in the channel obtained from the axi-symmetric model. The results are normalized to the pressure drop required in a pressure driven system for the same fluid outflow (Eq. 10). In the case of particles being used as fluid drivers, the pressure drop over the whole channel is distributed into multiple smaller pressure drops over each particle. The pressure drops are reduced further by the spreading of particles. The pressure reduction is proportional to the number of particles added to the system. In the case of a channel filled with evenly spaced particles, the required pressure can decrease to  $\sim 10\%$  of the pressure required in a pressure driven system.

#### 4.3 Driving fluids in perpendicular orientation

Particle chains that are oriented perpendicular to their motion direction have to be studied with the three-dimensional model. The velocity of a chain in this orientation increases as a function of its length  $l$ . If the channel radius compared to the chain length gets smaller, the ends of the chains approach the walls and slow down the entire chain, which can result in curved chains or even break-ups. The induced fluid outflow by chains in this configuration increases by adding more particles in the system as shown in Fig. 5d. However, particles that are not located on the channel axis experience more drag by the channel walls and therefore lower the pump efficiency. The increase in fluid outflow with the number of particles within the chain

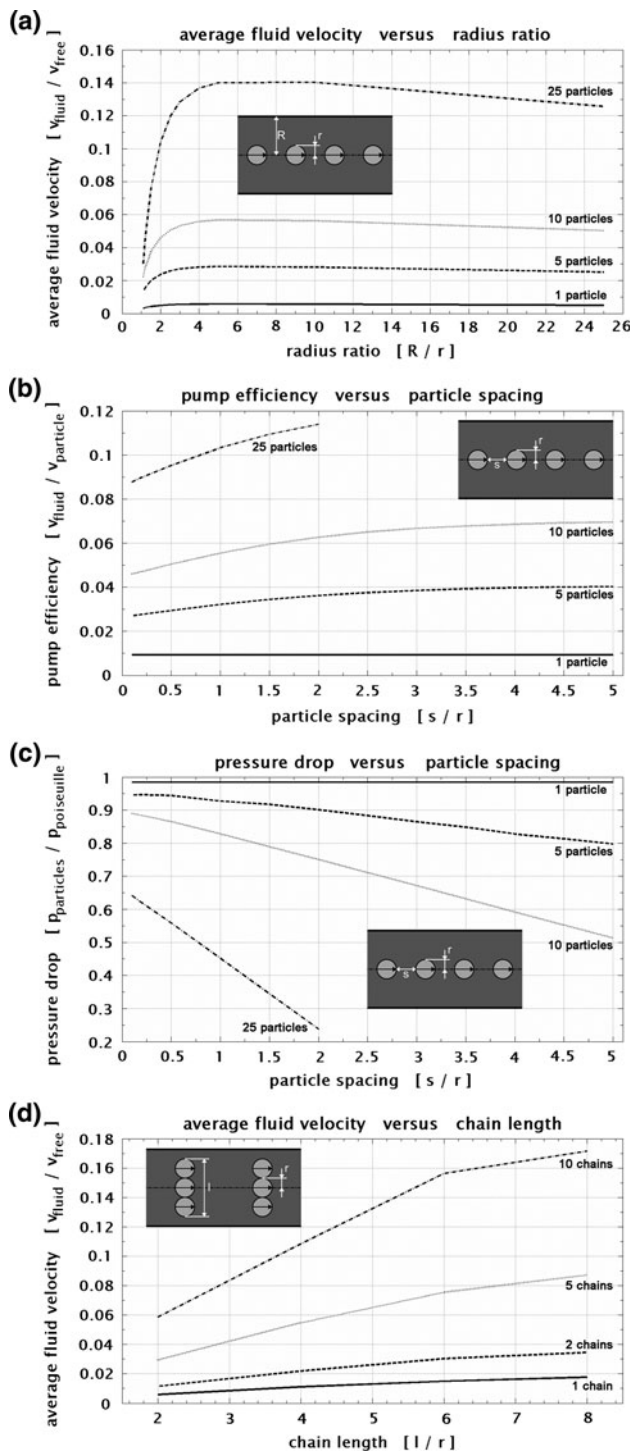


**Fig. 5** Numerical simulation results of the fluid flow induced by magnetic particles with radius  $r$ , traveling through a microchannel with radius  $R$  and length  $L = 100 \cdot r$ . With particles positioned along the axis, the highest fluid flow is reached at a radius ratio  $R/r$  between 5 and 10 (a). Equidistant spreading of the particles to  $s \geq 5 \cdot r$  enhances the particle pump efficiency defined as  $\bar{v}_f / \bar{v}_p$  (b), and reduces the internal pressure drops within the micro channel considerably (c). Adding more particles to a perpendicular chain increases the induced fluid outflow, but in this configuration the efficiency per particle is not as high as for particles aligned on the axis (d)

is less than proportional, as is the case of particle chains aligned along the channel axis. The contributions of more identical chains can still be linearly superimposed and does not depend on their interspacing.

### 5 Conclusion and outlook

In this paper, we studied magnetic particles to be used as integrated fluid drivers in microchannel systems. Since the channel and particle dimensions are almost similar, the system could not be considered as a continuum but the local particle-to-particle and particle-to-wall interactions determined the flow behavior and were therefore investigated in detail. Different particle configurations were visualized experimentally and evaluated numerically, which appeared to be influenced by the strong short-range magnetic interactions and the weaker but longer ranged hydrodynamic interactions. An experimental setup has been designed to study the particle motion, which is able to create an isodynamic magnetic force field over the microchannel. The design minimizes coupling between the magnetic and hydrodynamic interactions, by orienting the magnetic field lines perpendicular to the channel axis. In the experiments, particles reorganize by virtue of the changing balance between magnetic and hydrodynamic interactions. At low fields (10 mT in our case), the particles organize into an axially aligned and spread particle twin system. At high fields (50 mT in our case), the particles aggregate in chains oriented perpendicular to their motion direction.

Assuming the particles equilibrate instantaneously in a new stable configuration, numerical simulations could quantitatively predict the transition regime between axial and perpendicular alignments. The same simulations have shown that the highest fluid outflow is achieved with particles lined up on the channel axis, at a channel to particle radius ratio  $R/r$  ranging from 5 to 10. If the particles are spread out along the channel by  $s \geq 5 \cdot r$  the highest particle pump efficiency can be reached, where the fluid velocity can achieve more than 10% of the particles velocity. The spreading of particles lowers considerably the required pressure drop in the channel to only 10% of what is required in a pressure driven system. Particle chains in a perpendicular orientation increase the average fluid outflow, but the pump performance and efficiency per particle is lower compared to the case of axial configurations.

The integration of fluid actuation by magnetic particles in porous microsystems could be carried out using miniaturized current wires or soft magnetic field concentrators. In real applications, the pore structures are much shorter than in our experimental setup, so that only one regime and

resulting particle configuration will be present. In order to minimize the risk of clogging by particle agglomerates and optimize fluid outflow, the design should focus on high magnetic gradients and low field values to stimulate axial particle configurations. Perpendicular configurations could on the other hand enhance mixing near boundary walls where the fluid and analyte exchange is usually low. We will further study the observed focusing effects of off-axis particles and their rotational degree of freedom with the purpose to enhance chaotic advection. In addition to the use in open-ended channels, we foresee that integrated fluid actuation by magnetic particles can be used in dead-end micropore systems, where pressure-driven systems are completely ineffective for the exchange of fluids.

**Open Access** This article is distributed under the terms of the Creative Commons Attribution Noncommercial License which permits any noncommercial use, distribution, and reproduction in any medium, provided the original author(s) and source are credited.

## References

- Bruls D, Evers T, Kahlman J, Van Lankvelt P, Ovsyanko M, Pelssers E, Schleipen J, De Theije F, Verschuren C, Van Der Wijk T, Van Zon J, Dittmer W, Immink A, Nieuwenhuis J, Prins M (2009) Rapid integrated biosensor for multiplexed immunoassays based on actuated magnetic nanoparticles. *Lab Chip*, accepted
- Chalmers J, Zhao Y, Nakamura M, Melnik K, Lasky L, Moore L, Zborowski M (1999) An instrument to determine the magnetophoretic mobility of labeled, biological cells and paramagnetic particles. *J Magn Magn Mater* 194:231–241
- Chen X, Cui D, Liu C, Li H (2007) Fabrication of DNA purification microchip integrated with mesoporous matrix based on MEMS technology. *Microsyst Technol* 14:51–57
- Derks R, Dietzel A, Wimberger-Friedl R, Prins M (2007) Magnetic bead manipulation in a sub-microliter fluid volume applicable for biosensing. *Microfluid Nanofluid* 3:141–149
- Derks R, Frijns A, Prins M, Dietzel A (2008) Self-organized twinning of actuated particles for microfluidic pumping. *Appl Phys Lett* 92:024104
- Ganguly R, Zellmer B, Puri I (2005) Field-induced self-assembled ferrofluids aggregation in pulsatile flow. *Phys Fluid* 17:097104
- Gijs M (2004) Magnetic bead handling on-chip: new opportunities for analytical applications. *Microfluid Nanofluid* 1:22–40
- Grasso V, Lambertini V, Ghisellini P, Valerio F, Stura E, Perlo P, Nicolini C (2006) Nanostructuring of a porous alumina matrix for a biomolecular microarray. *Nanotechnology* 17:795–798
- Gutmann O, Kuehlewein R, Reinbold S, Niekrawietz R, Steinert C, De Heij B, Zengerle R, Daub M (2005) Fast and reliable protein microarray production by a new drop-in-drop technique. *Lab Chip* 5:675–681
- Haerberle S, Zengerle R (2007) Microfluidic platforms for lab-on-a-chip applications. *Lab Chip* 7:1094–1110
- Happel J, Brenner H (1973) *Low Reynolds number hydrodynamics—with special applications to particulate media*. Noordhoff International Publishing, Leyden
- Hartshorne H, Backhouse C, Lee W (2004) Ferrofluid-based microchip pump and valve. *Sens Actuators B* 99:592–600
- Hatch A, Kamholz A, Holman G, Yager P, Böhrringer K (2001) A ferrofluidic magnetic micropump. *J Microelectromech Syst* 10:215–221
- Laser D, Santiago J (2004) A review of micropumps. *Micromech Microeng* 14:35–64
- Mikkelsen C, Bruus H (2005) Microfluidic capturing-dynamics of paramagnetic bead suspensions. *Lab Chip* 5:1293–1297
- Mikkelsen C, Hansen M, Bruus H (2005) Theoretical comparison of magnetic and hydrodynamic interactions between magnetically tagged particles in microfluidic systems. *J Magn Magn Mater* 293:578–583
- Pamme N (2006) Magnetism and microfluidics. *Lab Chip* 6:24–38
- Petousis I, Homburg E, Derks R, Dietzel A (2007) Transient behavior of magnetic micro-bead chains rotating in a fluid by external fields. *Lab Chip* 7:1746–1751
- Van Ommering K, Lamers C, Nieuwenhuis J, Van IJzendoorn L, Prins M (2009) Analysis of individual magnetic particle motion near a chip surface. *J Appl Phys* 105:104905
- Vanderhoeven J, Papaert K, Dutta B, Van Hummelen P, Desmet G (2005) Comparison of a pump-around, a diffusion-driven, and a shear-driven system for the hybridization of mouse lung and testis total RNA on microarrays. *Electrophoresis* 26:3773–3779
- Yuen P, Guangshan L, Bao Y, Müller R (2003) Microfluidic devices for fluidic circulation and mixing improve hybridization signal intensity on DNA arrays. *Lab Chip* 3:46–50